

Planar-integrated Talbot array illuminators

Markus Testorf and Jürgen Jahns

We demonstrate the planar integration of Talbot array illuminators designed to generate one-dimensional spot arrays. The array illuminator basically consists of a phase grating and a cylindrical diffractive lens integrated as a single diffractive optical element onto a transparent glass substrate. We discuss various design aspects, and we focus on problems typical for planar-integrated free-space optics like the tilted optical axis of the system. Experimental results and measurements, which were obtained from planar-integrated setups fabricated as surface-relief structures on a transparent glass substrate by use of standard photolithography, are included. © 1998 Optical Society of America

OCIS codes: 050.0050, 050.1380, 070.0070, 070.6760, 350.3950.

1. Introduction

One of the most important applications of diffractive optics is array illuminators, i.e., optical systems that are able to concentrate the light intensity of a continuous wave front into an array of bright spots or narrow beams.^{1,2} Probably best known is array generation with computer-generated Fourier holograms, which form the desired spot array in the Fraunhofer diffraction plane.^{3–5} Alternative methods based on spatial filtering are array generation with microlens arrays⁶ or phase-contrast imaging of phase-only gratings.⁷ A good survey of the different concepts for array generation can be found in Ref. 1.

Among the known methods for generating spot arrays or narrow beams, Talbot array illuminators (TAI's) are very attractive because the spot pattern is formed by free-space diffraction of the wave front behind a phase-only diffraction grating.² No additional element or alignment is required. Typically, all spots have the same phase, and the array illuminator is scaleable, i.e., more spots can be generated by extension of the diffraction grating. In theory, the efficiency increases with the number of spots, which, however, requires an ideal incident plane wave front. The dependence of the output spot array on the illu-

minating wave front⁸ can be a serious problem if a high homogeneity of the spots is required. Therefore TAI's are better suited for applications in which the complexity of the optical system is a major concern rather than the homogeneity of the spot pattern. Because the possibility of array generation by use of the fractional Talbot effect was proposed,² a large variety of gratings suitable for generating spot arrays with different properties and geometries was investigated and experimentally characterized (see, e.g., Refs. 9–12). This includes array generation with several layers of binary phase gratings, which was proposed recently.¹³

In this paper we focus on the planar integration of TAI's. In this context planar integration refers to free-space micro-optical systems that are folded into a plane-parallel transparent substrate.^{14,15} All elements are located at the surfaces, where they form a two-dimensional structure that can be integrated as a single diffractive optical element by standard lithographic techniques compatible with those used in microelectronics.

The specific geometry of planar optical systems usually requires additional efforts with respect to the design compared with conventional optical systems. For instance, the locations of elements at the surface of the substrate limit the range within which the distance between elements can be chosen. In addition, even for a paraxial design, modifications of the parabolic approximation have to be taken into account because of the tilted optical axis of the integrated system.¹⁶ Although we specifically investigate the integration of TAI's, our considerations are not limited to this application and illustrate general ideas about the design of planar-integrated systems.

In Section 2 we describe the basic setup and the

When this study was performed, the authors were with Optische Nachrichtentechnik, FernUniversität Hagen, Feithstrasse 140, 58084 Hagen, Germany. M. Testorf is now with the Department of Electrical and Computer Engineering, University of Massachusetts-Lowell, One University Avenue, Lowell, Massachusetts 01854.

Received 23 February 1998; revised manuscript received 8 May 1998.

0003-6935/98/235399-09\$15.00/0

© 1998 Optical Society of America

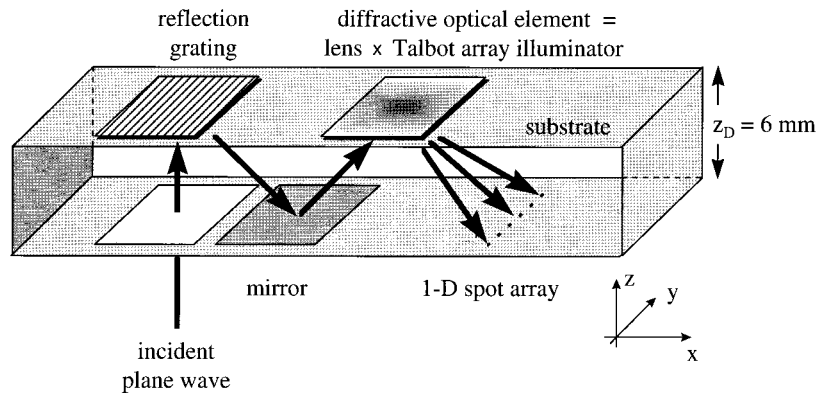


Fig. 1. Basic configuration of a planar-integrated TAI. A plane wave is converted into a 1-D spot array. The input and the output planes are located on the bottom surface of a transparent glass substrate.

desired properties of the array illuminator, as well as of the planar system. The design is split into parts, and we first, in Section 3, discuss the design of the cylindrical lens. In Section 4 we concentrate on the TAI. In Section 5 the deflection angle is shown to provide the freedom necessary to achieve the correct propagation distance for generating the spot array. Finally, Section 6 contains information on the realization of the system as a quantized surface-relief element. This includes measurements of the output spot array, which are compared with the theoretical performance.

2. Scheme of the Planar-Integrated System

The basic planar-integrated setup we want to investigate is shown in Fig. 1. A plane wave incident perpendicular to the bottom surface is reflected and redirected by a reflection grating. After an additional reflection at the bottom surface the diffractive optical element for beam shaping is illuminated. This element consists of a diffractive cylindrical lens in the x direction that forms a focal line. Superimposed on the lens is a one-dimensional (1-D) phase grating oriented in the y direction, which modulates the focal line and forms a 1-D spot array at the bottom surface of the substrate.

The tilted optical axis of the folded planar system is known to cause aberrations of TAI's.¹⁷ Therefore the 1-D spot array is oriented in the direction perpendicular to the tilt, for which the shape of the spots is not affected by these aberrations. For collimation of the plane wave into a single focal line it is possible to find an ideal shape of the diffractive lens that compensates for the tilted optical axis.

All elements of the system are manufactured as a single diffractive structure by use of binary-optics technology.¹⁸ For this project we were restricted to a design with four discrete phase levels, fabricated with two mask layers and two corresponding cycles of the photolithographic process. This also implies that the superposition of the lens and the TAI grating must again form a diffractive structure of four levels.

The minimum feature size of the fabrication process is $\delta r = 0.7 \mu\text{m}$, and the demonstration setup was

designed for a wavelength of $\lambda = 0.633 \mu\text{m}$, which provides the possibility of working with visible light. The substrate is silica glass with a refractive index of $n = 1.457$ and a thickness of $z_D = 6 \text{ mm}$. Consequently, the maximum diffraction angle $\arcsin(\lambda/n2\delta r)$ is limited to 18° , which is also the upper bound for the tilt angle of the optical axis in Fig. 1. We chose the spot distance, which is equal to the grating period of the TAI, to be $d = 65.5 \mu\text{m}$. This value was taken from the requirements of another project on array generation to provide realistic conditions.

To study the potential that planar integration provides for Talbot array generation, we do not discuss a single design but rather four different setups, which are shown in Fig. 2. System 1 is equivalent to the basic setup in Fig. 1. In system 2 the diffractive lens includes a diffractive prism to increase the range for the propagation angle α beyond 18° . Similarly, an additional deflection grating is incorporated into the lens of system 3 to achieve a propagation angle at the output that is perpendicular to the surface of the substrate. This might be necessary, e.g., if the spot intensity were received by a detector array with a limited numerical aperture oriented accordingly. Compared with this situation, systems 1 and 2 are better suited for applications in which the spot array is part of a more complex system and the light signal propagates farther along a zig-zag path inside the substrate. System 4 contains two separated elements for collimation and redirection to decrease the required resolution for each of the elements.

3. Design of the Diffractive Cylindrical Lenses

Theoretically, the problem of focusing a tilted plane wave can be solved uniquely. For a cylindrical lens the phase of the transmittance function is given by¹⁹

$$\phi_{\text{oa}}(x) = -\frac{2\pi}{\lambda} n \{ [x^2 + f^2 - 2xf \sin(\alpha)]^{1/2} + x \sin(\alpha) \}, \quad (1)$$

where α is the deflection angle, n is the refractive index, and f is the focal distance counted along the tilted optical axis (oa). Because this profile is highly

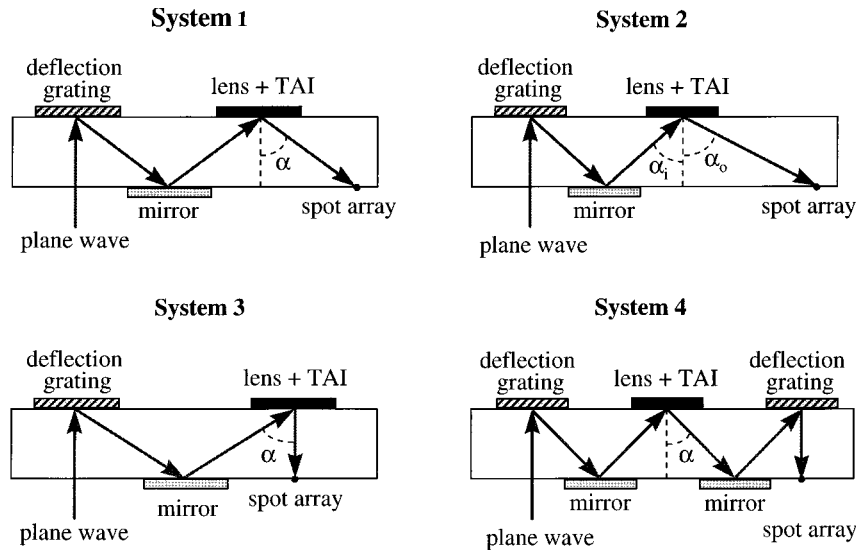


Fig. 2. Geometries of the planar-integrated systems investigated.

specialized to an ideal configuration, other phase profiles are better suited to provide tolerance against variations of the wave front and the angle of incidence of the illuminating beam. Alternatively, the symmetrical counterpart of the profile in Eq. (1) (Ref. 20) or even a parabolic lens¹⁶ can be used.

The particular phase functions we employed are listed in Table 1. For systems 1 and 2, in Fig. 2, we used the symmetrical lens profile, whereas for system 3 the profile deriving from Eq. (1) was applied. For system 4 we implemented the parabolic lens profile. In systems 2 and 3 the phase function contains an additional phase wedge to redirect the converging beam. In system 4 redirection by the second deflection grating has to be considered by a modified focal distance. The phase functions in Table 1 are expressed in terms of the thickness z_D of the substrate to relate the lens shape to the predefined parameters of the system.

To implement the continuous-phase distribution as a discrete diffractive element, we apply the well-known quantization rules for diffractive lenses: the

diffractive structure is quantized into discrete, equidistant phase levels between 0 and 2π . For L phase levels the discrete values are, namely,

$$\phi_l = \frac{2\pi}{L} l, \quad l = 0, 1, \dots, L - 1, \quad (2)$$

where L is a power of 2, i.e., $ld(L)$ corresponds to the number of mask patterns necessary to fabricate the diffractive element. The transition points are identical to the spatial coordinates where the continuous phase function equals the discrete phase levels. This can be shown to introduce minimum quantization errors.²¹

The minimum feature size of the quantized structure determines the achievable numerical aperture of the lens. The lens apertures used for the systems shown in Fig. 2 are included in Table 1 and correspond to the available numerical aperture. In system 3, however, the minimum feature size drops below $0.7 \mu\text{m}$ because of the additional phase wedge.

Table 1. Design Parameters of the Diffractive Cylindrical Lenses

	Phase of the Transmission Function	Lens Aperture (mm)	Deflection Angle
System 1	$\phi(x) = -\frac{\pi}{\lambda} \left[\left(x^2 + \frac{z_D^2}{\cos^2 \alpha} - 2xz_D \tan \alpha \right)^{1/2} + \left(x^2 + \frac{z_D^2}{\cos^2 \alpha} + 2xz_D \tan \alpha \right)^{1/2} \right]$	1	$\alpha = 13.6^\circ$
System 2	$\phi(x) = -\frac{\pi}{\lambda} \left[\left(x^2 + \frac{z_D^2}{\cos^2 \alpha_o} - 2xz_D \tan \alpha_o \right)^{1/2} + \left(x^2 + \frac{z_D^2}{\cos^2 \alpha_o} + 2xz_D \tan \alpha_o \right)^{1/2} \right] - \frac{2\pi}{\lambda} (\sin \alpha_o - \sin \alpha_i)$	0.5	$\alpha_i = 12.5^\circ$ $\alpha_o = 24.3^\circ$
System 3	$\phi(x) = -\frac{2\pi}{\lambda} [(x^2 + z_D^2)^{1/2} + x \sin \alpha]$	0.75	$\alpha = 10^\circ$
System 4	$\phi(x) = -\frac{\pi}{\lambda z_D} \left(\frac{2}{\cos^3 \alpha} + 1 \right)^{-1} x^2$	2	$\alpha = 16.5^\circ$

Table 2. Optimum Design of TAI's with Four Equidistant Phase Levels

	Working Distance $z = M/N z_T$	Number of Features per Period	Phase Values ($\pi/2$)	Spot Size (δ/d)	Efficiency of Infinite Grating
System 1	$N = 15, M = 5$	8	0 - 1 - 3 - 0 - 3 - 3 - 1	1/8	96%
System 2	$N = 3, M = 1$	3	1 - 0 - 0	1/3	94%
System 3	$N = 10, M = 3$	5	0 - 0 - 2 - 3 - 2	1/5	92%
System 4	$N = 16, M = 15$	8	0 - 0 - 1 - 2 - 0 - 2 - 1 - 0	1/8	96%

In this special case we accepted features as small as to 0.5 μm .

As we discuss in Section 4, the deflection angles in Table 1 cannot be chosen freely because the TAI requires a well-defined propagation distance of the light signal to form the spot array. Only the angles α_i in system 2 and α in system 3 do not influence the propagation distance between the TAI and the output plane and were chosen arbitrarily.

4. Phase-Only Gratings for Array Generation

The basic setup of a TAI consists of a phase-only grating that is illuminated by a plane wave. The diffracted wave front forms the desired spot pattern at a distance

$$z_F = \frac{M}{N} \frac{2d^2}{\lambda}. \quad (3)$$

Pattern formation can be understood in terms of the fractional Talbot effect, which is equivalent to Fresnel diffraction at the rational fraction M/N of the so-called Talbot distance $z_T = 2d^2/\lambda$. Here, d is the grating period and N and M are integer numbers. The diffraction amplitude in a fractional Talbot plane can be calculated from a superposition of N copies of the transmission function of the grating for which each copy is shifted by an integer multiple of d/N and modulated by a constant complex factor.²²

Typically, spatially quantized groove shapes are considered for TAI's in which a single period consists of Q pixels of equal size (see, e.g., Ref. 23). With Q features a spot size of $\delta = d/Q$ can be achieved. Then, for N odd, the spot pattern can be picked up at planes $N = Q$, whereas for N even the corresponding diffraction planes are those with $N = 2Q$.

Although substructured Talbot gratings are compatible with binary optics in the sense that the spatially quantized elements automatically consist of a finite set of discrete phase levels, the number of required phase levels typically increases with a decreasing spot-size ratio δ/d . This problem becomes even more severe if equidistant phase steps in the range $[0, \dots, 2\pi]$ are required.

As an example that illustrates this problem, we refer to a design described in Ref. 10 in which the discrete phase levels of the TAI take the values

$$\phi_q = \pi \frac{q^2}{Q}, \quad q = -Q/2, \dots, Q/2 - 1. \quad (4)$$

The corresponding diffraction plane is given by $M = 1$ and $N = 2Q$. To count the number L according to Eq. (2), which is necessary to include all phase values in Eq. (4) as a subset of the equidistant set of phase levels, we consider only the case for which Q is a power of 2 and find $L = 2Q$. Thus the four-level design of the planar-integrated TAI is limited to a spot size of $d/2$, which is a very strong limitation for practical applications. The constraint of equidistant phase levels also excludes designs that provide a larger compression ratio, even by use of binary phase-only gratings, but with phase steps not matching those in Eq. (2).^{9,13}

We note that most Talbot gratings including those of Eq. (4) are designed to yield a 100% efficiency for an ideal, infinitely extended grating, i.e., all the intensity is diffracted into the desired spots. More recently, however, the idea was proposed to achieve spot-array generation with a small spot size by means of trading the efficiency against the number of phase levels.²⁴

To overcome the problem of a limited ratio δ/d , we combine this idea with the concept of numerical optimization of diffractive optical elements. The design of a TAI can be considered an optimization problem for which the groove shape of a discretized phase-only grating has to be determined such that the intensity in the fractional Talbot plane yields the desired spot pattern or at least the optimum efficiency.

For the planar-integrated TAI we explored spot sizes as small as $d/8$. For four discrete phase levels all possible combinations of phase values can be tested to select the global optimum. On a 200-MHz Pentium PC the calculation of the optimum phase distribution takes a few minutes only. For higher compression ratios or a larger set of phase levels the optimum design has to be obtained by a numerical optimization algorithm to reduce the number of calculated phase distributions. A more detailed description of this approach is given elsewhere.²⁵

The TAI's we used for the four different integrated systems are summarized in Table 2. The values for the efficiency refer to the ratio of the intensity diffracted into the desired spots and the total intensity, assuming diffraction at an infinite grating under the paraxial approximation. The examples in Table 2 prove that a significant reduction of the spot size can be achieved if the efficiency is kept to better than 90%, even with a four-level design.

The lost light enters the output pattern as back-

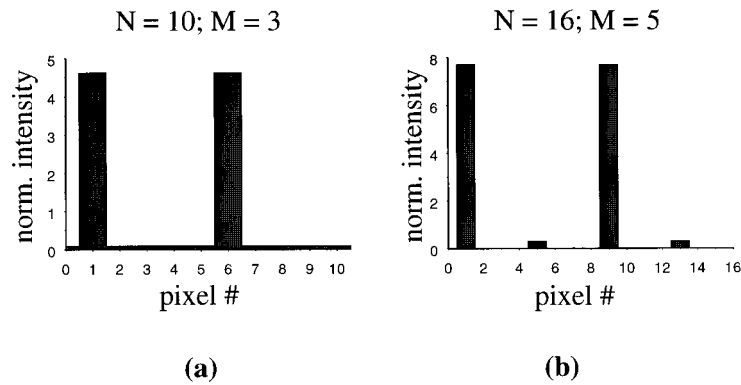


Fig. 3. Theoretical intensity profiles for the TAI's listed in Table 2.

ground intensity. The designs we used show two different behaviors. For systems 1 and 2 a uniform background is formed. As an example, the ideal intensity pattern of system 1 is shown in Fig. 3(a). In systems 3 and 4 the desired spots are interlaced with unwanted spots of low intensity [Fig. 3(b)].

The particular fractional Talbot plane M was selected to generate the spot pattern at the bottom surface of the glass substrate and to keep the deflection angle within acceptable limits. M has to be determined in conjunction with the deflection angle.

5. Deflection Angle as a Degree of Freedom

For a fixed thickness z_D of the glass substrate the effective propagation distance of the light signal between the array illuminator and the spot pattern is determined by the deflection angle of the optical axis. For a given spot size of $\delta = d/Q$ there are two degrees of freedom, which can be used to generate the spot array at the bottom surface or any other desired location. Besides the deflection angle, this is the choice of the plane M .

Both parameters are bounded: With increasing M the influence of the walk-off effect, i.e., the diffraction at the finite aperture of the grating, increases and degrades the quality of the spot array.²⁶ The tilt angle of the optical axis, or more precisely, the change of the angular spectrum that can be achieved, is limited by the resolution of the lithographic fabrication process, as mentioned above.

The relation between the tilt angle and the desired diffraction plane M can be found by rewriting the expression for the fractional Talbot distance. For system 1 (Fig. 2) we get²⁷

$$\cos \alpha = \frac{N z_D \lambda}{M 2d^2}. \quad (5)$$

Equation (5) also holds for system 2 when $\alpha = \alpha_o$ is substituted in. For system 3 the deflection angle between the TAI and the spot array is 0, and in general Eq. (5) can be fulfilled only approximately. For system 4 the propagation distance between the array illuminator and the output plane is split into an α -dependent part and a part for which the light signal

propagates perpendicular to the surface. We get the modified relation

$$\cos \alpha = \left(\frac{M 2d^2}{N z_D \lambda} - 1 \right)^{-1}. \quad (6)$$

For every system we can now calculate all possible combinations of α and the integer M . From these combinations we selected examples for which $M < N$ and α lies between 10° and 25° . The specific values for α are included in Table 1. For system 3, for which no exact match can be obtained, the fractional Talbot plane nearest to the bottom surface was chosen.

6. Experiment Results

The four systems as discussed above were fabricated by a standard photolithographic process. The two binary amplitude masks were generated by e -beam lithography on a chromium layer. The diffractive surface reliefs were then fabricated by a two-step photolithographic process in which each step involves copying of the chromium mask into a photoresist structure and transferring the photoresist structure to the glass substrate by means of reactive-ion etching. The surface was finally covered with a layer of aluminum to use the diffractive elements in reflection.

For working in reflection, the minimum step size in the surface-relief structure necessary to obtain a phase shift of $\pi/2$ for a wavelength of $\lambda = 0.633 \mu\text{m}$ and a refractive index of $n = 1.457$ is approximately 50 nm. Because the etching rate is hard to control for this small step size, as opposed to larger steps, the etch depth of the complete structure was biased by an additional phase step of 2π .

A top view of the substrate is shown in Fig. 4(a). From the enlarged picture of the array illuminator of system 4 [Fig. 4(b)], the linear grating structure in one direction as well as the pattern of the cylindrical lens in the other direction can be recognized. Figure 4(c) shows a section of the array illuminator of system 3. Because of the minimum feature size of $0.5 \mu\text{m}$ that the structure was designed for, fabrication errors can be recognized in the high-frequency structure in the x direction.

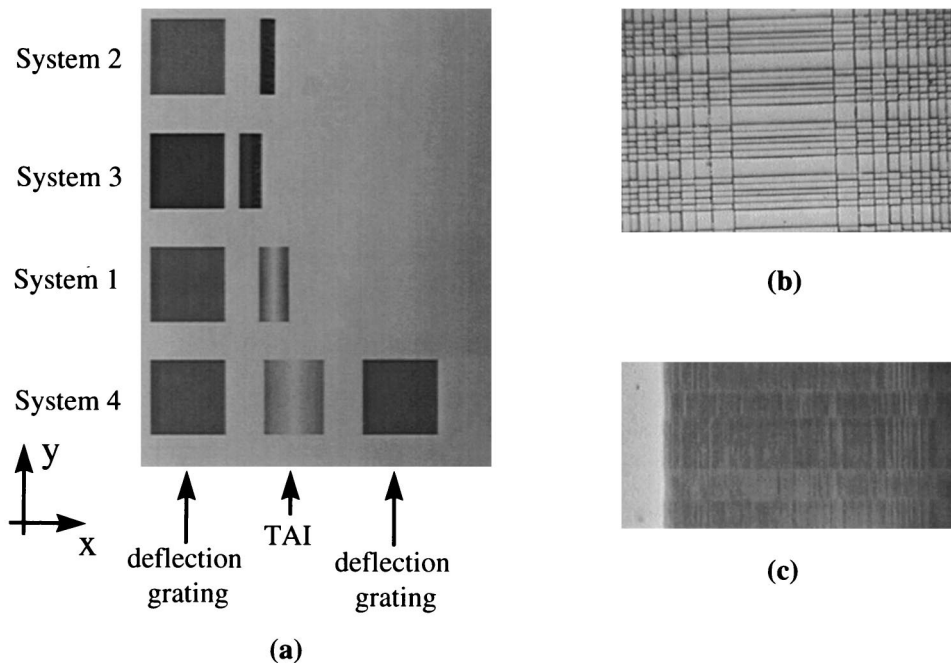


Fig. 4. (a) CCD camera pictures of the planar-integrated systems. (b) Enlarged picture of the array illuminator of system 4. (c) Section of the array illuminator of system 3.

For characterizing the planar-integrated systems the input window was illuminated with an expanded and collimated laser beam. The output was investigated by a microscope lens that imaged the intensity pattern onto a CCD camera. As an example, Fig. 5(a) shows the output spot pattern of system 4, as generated on the surface of the glass substrate. The intensity pattern shows the typical behavior of a TAI: In the central area the spot intensity is quite homogeneous, whereas toward the edge of the spot array a strong intensity modulation can be observed.

This modulation is caused by diffraction at the finite window of the array illuminator and by an ad-

ditional intensity modulation of the incident beam that cannot be avoided completely. For specific applications, perhaps spatially resolved sensing might be useful. In this case a distinct modulation can be further achieved by the combination of the TAI with a customized system for additional beam shaping.

From the overexposed picture of the spot array [Fig. 5(b)] the designed intensity pattern of the TAI can be verified qualitatively: between the desired spots interlaced spots of low intensity can be encountered. These low-intensity spots correspond to the background intensity of the design shown in Fig. 3(b).

We also recorded line scans of the output intensity

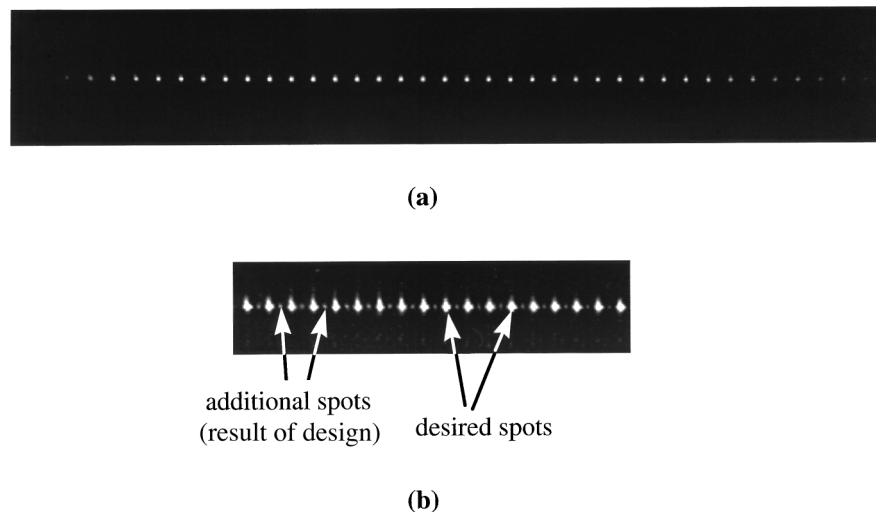


Fig. 5. (a) Intensity pattern of the spot array generated by system 4. (b) Interlaced spots of low intensity can be found in the overexposed camera picture.

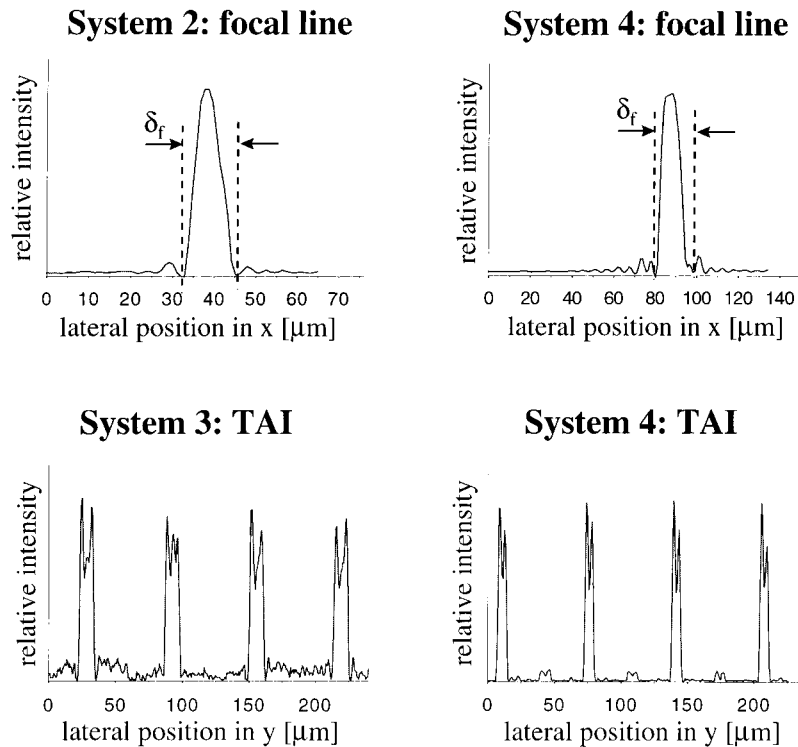


Fig. 6. Examples of 1-D line scans through both the focal line of the cylindrical lenses and the spot arrays.

patterns. Figure 6 contains four examples that are best suited to illustrate the properties of the spot arrays. Scans through the focal line of the cylindrical lenses basically correspond to the well-known sinc^2 pattern. For system 4, however, the structure of both sidelobes shows rapid oscillations caused by diffraction at the aperture of the second deflection grating (Fig. 2).

The linewidth of the focal line, i.e., the distance between the first minima of the intensity pattern, was measured and compared with the diffraction-limited value (Table 3). The theoretical values were estimated from the design parameters of Table 1 on the basis of a paraxial analysis.¹⁶ The deviations between theoretical values and measurements are caused by several effects: The strong deviation for system 1 is caused partially by the CCD camera for data acquisition, because the small size of the focal line becomes comparable with the resolution of the camera system. An additional effect is the curvature of the input wave front, which can never be completely avoided. Systems 1 and 3 with a small

focal line, i.e., a small depth of focus, are affected more severely.

System 3 also suffers from the imperfect fabrication of the high-frequency structures of the array illuminator [Fig. 4(c)]. The effective lens aperture is smaller than that in the theoretical design. The deviation in system 4 is due mainly to the specific modulation of the right sidelobe (Fig. 6). The first minimum does not appear, and instead the second minimum was taken to determine the linewidth. The width of the central peak, however, is close to the diffraction-limited width. An almost perfect match is found for system 2, which indicates that the extension of the deflection angle by an integrated design can be done as long as the resulting structures do not violate the constraints of the fabrication process.

From our results it is not possible to make a final judgment on the optimum shape for a planar-integrated collimation lens. The optimum design, of course, depends on the trade-off between optimum collimation of a specific wave front and a certain tolerance to wave-front aberrations. However, further

Table 3. Comparison of Theoretical and Experimental Results

	Diffraction-Limited Line Diameter δ_f (μm)	Measured Line Diameter δ_f (μm)	Efficiency of Infinite Grating	Measured Efficiency per Period (Central Part)
System 1	5.7	10	96%	89%
System 2	13.8	16	94%	92%
System 3	7.0	12	92%	85%
System 4	11.8	17	96%	90%

investigations are necessary to define the conditions under which optimization is worth the effort.

We also investigated line scans along the spot arrays. For the central part of the array we calculated the ratio of intensity in the desired spot locations and the total intensity within one period. In Table 3 these values are compared with the theoretical values of an infinite grating. The measured efficiency is 2%–7% below the theoretical value. The small value for system 3 is again caused by imperfections of the diffractive element. This also explains the strong background in Fig. 6, which is significantly stronger than expected from the design (Fig. 3). The line scan of system 3 recorded at the surface of the substrate indicates that the depth of focus is large enough to preserve the rectangular shape of the spots, even if no exact match with a fractional Talbot plane can be found.

The other values indicate a certain dependency of the efficiency on the compression ratio δ/d . For larger spots, light that is diffracted off the desired location still has a high probability of being within the area of the spot. This also explains the excellent value obtained for system 2. The line scan of system 4 again shows interlaced spots of low intensity. Both line scans along the spot arrays in Fig. 6 show an additional modulation of the spots that is another effect of the diffracting aperture of the grating.

We also determined the homogeneity and the total efficiency of the spot arrays. These, however, strongly depend on the quality of the input wave front and should be regarded as only estimates. Typically, we found the maximum deviation of the spot intensity to be smaller than 3% for half the initial grating size. The total efficiency of the TAI's was obtained as the ratio of the intensity of all spots with a maximum deviation of 5% from the mean intensity value and the total intensity along the recorded line. As typical values, we found efficiencies of approximately 70%–80%.

7. Conclusions

In this paper we have demonstrated the planar integration of TAI's. The considerations necessary to the design of the optical systems illustrate typical problems that arise from a planar integration of free-space optics. For instance, we have discussed the quantization of the diffractive structures of the system into diffractive elements with equidistant phase levels to reduce the number of masks in the fabrication process. For the particular problem of integrated TAI's, we have developed an optimization method to find the optimum solution that trades the complexity versus the efficiency of the structure.

As an additional problem typical for planar-integrated optics, we have discussed how the tilt angle of the optical axis has to be used as a degree of freedom to obtain distinct propagation distances in the fixed geometry of plane-parallel substrates.

Our experimental results have showed that any design of a planar-integrated system is strictly limited by the available space–bandwidth product,

which depends on the resolution of the fabrication process. Our results have further indicated that, within these bounds, the freedom diffractive optics provides for the design can be used entirely. This includes the integration of a collimation lens and a deflection grating into a single element to extend the range of the tilt of the optical axis. Alternatively, a more conservative design in which all tasks are performed by individual elements yields similar results. For planar-integrated systems both designs can be realized by the same number of fabrication steps.

The experimental results have further proved that TAI's can successfully be integrated as planar-integrated systems that combine the simple concept of array generation with the compact integration concept of planar optics. This offers access to integrated systems for sensing applications that are based on the Talbot effect. Examples are integrated Talbot interferometers or spot projectors for distance measurement. Planar integration makes these systems attractive for small-scale applications.

The authors gratefully acknowledge the assistance of B. Wdowiak in the fabrication of the planar-integrated system. This research was financially supported by the Deutsche Forschungsgemeinschaft (DFG). Parts of this study were presented at the Annual Meeting of the Optical Society of America, 12–17 October 1997, Long Beach, California.

References and Note

1. N. Streibl, "Beam shaping with optical array generators," *J. Mod. Opt.* **36**, 1559–1573 (1989).
2. A. W. Lohmann, "An array illuminator based on the Talbot effect," *Optik (Stuttgart)* **79**, 41–45 (1988).
3. H. Dammann and K. Görtler, "High-efficiency in-line multiple imaging by means of multiple phase holograms," *Opt. Commun.* **3**, 312–315 (1971).
4. J. Mait, "Design of binary-phase and multiphase Fourier gratings for array generation," *J. Opt. Soc. Am. A* **7**, 1514–1528 (1990).
5. H. Machida, J. Nitta, A. Seko, and H. Kobayashi, "High-efficiency fiber gratings for producing multiple beams of uniform intensity," *Appl. Opt.* **23**, 330–332 (1984).
6. N. Streibl, U. Nölscher, J. Jahns, and S. Walker, "Array generation with lenslet arrays," *Appl. Opt.* **30**, 2739–2742 (1991).
7. A. W. Lohmann, J. Schwider, N. Streibl, and J. Thomas, "Array illuminator based on phase contrast," *Appl. Opt.* **27**, 2915–2921 (1988).
8. L. Liu, "Talbot and Lau effects on incident beams of arbitrary wavefront, and their use," *Appl. Opt.* **28**, 4668–4677 (1989).
9. A. W. Lohmann and J. A. Thomas, "Making an array illuminator based on the Talbot effect," *Appl. Opt.* **29**, 4337–4340 (1990).
10. J. R. Leger and G. J. Swanson, "Efficient array illuminator using binary-optics phase plates at fractional Talbot planes," *Opt. Lett.* **15**, 288–290 (1990).
11. H. Hamam, "Talbot array illuminators: a general approach," *Appl. Opt.* **36**, 2319–2327 (1997).
12. V. Arrizón and J. Ojeda-Castañeda, "Multilevel phase gratings for array illuminators," *Appl. Opt.* **33**, 5925–5931 (1994).
13. H. Hamam and J. L. de Bougrenet, "Multilayer array illuminators with binary phase plates at fractional Talbot distances," *Appl. Opt.* **35**, 1820–1826 (1996).

14. J. Jahns and A. Huang, "Planar integration of free space optical components," *Appl. Opt.* **28**, 1602–1605 (1989).
15. J. Jahns, "Planar packaging of free-space optical interconnections," *Proc. IEEE* **82**, 1623–1631 (1994).
16. M. Testorf and J. Jahns, "Paraxial theory of planar integrated systems," *J. Opt. Soc. Am. A* **14**, 1569–1575 (1997).
17. M. Testorf, J. Jahns, N. A. Khilo, and A. M. Goncharenko, "Talbot effect for oblique angle of light propagation," *Opt. Commun.* **129**, 167–172 (1996).
18. G. J. Swanson and W. B. Veldkamp, "Diffractive optical elements for use in infrared systems," *Opt. Eng.* **28**, 605–608 (1989).
19. T. Shiono and H. Ogawa, "Diffraction-limited blazed reflection diffractive microlenses for oblique incidence fabricated by electron-beam lithography," *Appl. Opt.* **30**, 3643–3649 (1991).
20. J. Jahns and B. Acklin, "Integrated planar optical imaging system with high interconnection density," *Opt. Lett.* **18**, 1594–1596 (1993).
21. U. Krackhardt, "Optimum quantization rules for computer generated holograms," in *Diffractive Optical Elements: Design, Fabrication, and Testing*, Vol. 11 of OSA Technical Digest Series (Optical Society of America, Washington, D.C., 1994), pp. 139–142.
22. J. T. Winthrop and C. R. Worthington, "Theory of Fresnel images. I. Plane periodic objects in monochromatic light," *J. Opt. Soc. Am.* **55**, 373–381 (1965).
23. V. Arrizón and J. Ojeda-Castañeda, "Multilevel phase gratings for array illuminators," *Appl. Opt.* **33**, 5925–5931 (1994).
24. V. Arrizón and J. G. Ibarra, "Trading visibility and opening ratio in Talbot arrays," *Opt. Commun.* **112**, 271–277 (1994).
25. Further research investigates nonlinear numerical optimization methods to calculate optimized TAI structures. The optimization procedure can be understood mainly as a quantization algorithm for ideal TAI gratings.
26. K. Patorski, "The self-imaging phenomenon and its applications," *Progress in Optics*, in E. Wolf, ed. (North-Holland, Amsterdam, 1989), Vol. XXVII, pp. 1–108.
27. M. Testorf, J. Jahns, N. A. Khilo, and A. M. Goncharenko, "Talbot effect for oblique angle of light propagation," *Opt. Commun.* **132**, 205–211 (1996).